

Hierarchical Memory Learning for Fine-Grained Scene Graph Generation

Youming Deng¹, Yansheng Li^{*1}, Yongjun Zhang¹, Xiang Xiang³, Jian Wang²,
Jingdong Chen², and Jiayi Ma¹

¹ Wuhan University

{`rename_deng,yansheng.li,zhangyj,jiayima`}@whu.edu.cn

² Ant Group

{`bobblair.wj,jingdongchen.cjd`}@antgroup.com

³ Huazhong University of Science and Technology

`xxiang@cs.jhu.edu`

Abstract. As far as Scene Graph Generation (SGG), coarse and fine predicates mix in the dataset due to the crowd-sourced labeling, and the long-tail problem is also pronounced. Given this tricky situation, many existing SGG methods treat the predicates equally and learn the model under the supervision of mixed-granularity predicates in one stage, leading to relatively coarse predictions. In order to alleviate the negative impact of the suboptimum mixed-granularity annotation and long-tail effect problems, this paper proposes a novel Hierarchical Memory Learning (HML) framework to learn the model from simple to complex, which is similar to the human beings’ hierarchical memory learning process. After the autonomous partition of coarse and fine predicates, the model is first trained on the coarse predicates and then learns the fine predicates. In order to realize this hierarchical learning pattern, this paper, for the first time, formulates the HML framework using the new Concept Reconstruction (CR) and Model Reconstruction (MR) constraints. It is worth noticing that the HML framework can be taken as one general optimization strategy to improve various SGG models, and significant improvement can be achieved on the SGG benchmark (i.e., Visual Genome).

Keywords: Scene Graph Generation, Mixed-Granularity Annotation, Hierarchical Memory Learning

1 Introduction

The task of Scene Graph Generation (SGG) [54] is a combination of visual object detection and relationship (i.e., predicate) recognition between visual objects. It builds up the bridge between computer vision and natural language. SGG receives increasing attention since an ideal informative scene graph has a huge potential for various down-stream tasks such as image caption [18,57] and

^{*} Yansheng Li is the corresponding author.

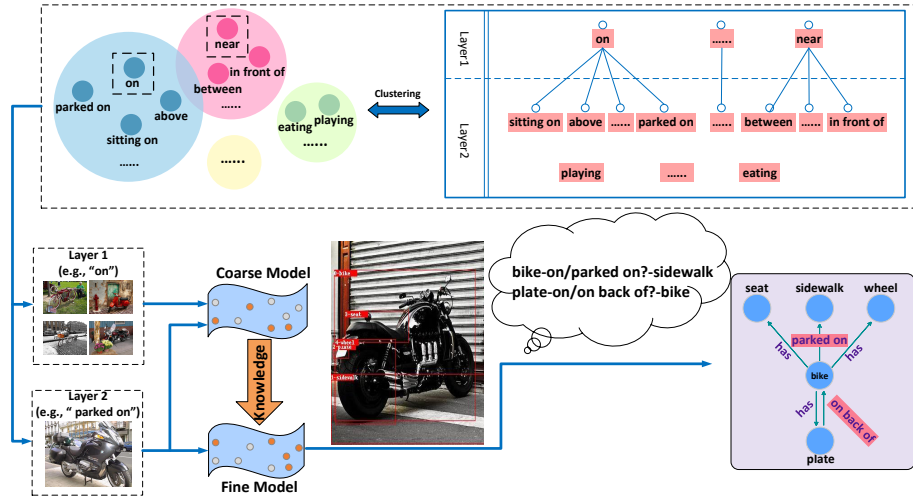


Fig. 1: **Automatic Predicate Tree Construction and visualization of the HML Framework.** After constructing a hierarchical predicate tree via clustering, the model is trained with the HML framework to make the fine-grained predicate prediction.

VQA [1,34]. To pursue the practical application value, SGG models keep working towards the generation of an informative scene graph where the fine-grained relationship between two objects should be predicted. Earlier works like [48,56,60] only design models for feature refinement and better representation. However, they ignore the dataset and task properties, limiting the performance. In order to deal with the long-tail effect and various biases [47] within the dataset, recent works including [7,17,43,47] move towards designing the learning framework (i.e., the optimization strategy) to improve the overall performance of several classic SGG models. Even with these progress, making the fine-grained predicate prediction is still challenging.

Generally speaking, two factors lead to frustrating result. The first is the mixed-granularity predicates caused by artificial subjective annotation. The predicate recognition in the dataset is much trickier than the image classification tasks. For instance, although Microsoft coco [32] has super categories, it does not require a model to have the ability to make a different prediction like “bus” and “vehicle” for a visually identical object. However, in the SGG task, a more general predicate like “on” and a more informative one like “parked on” will be learned and predicted simultaneously. Under this training condition, it is a dilemma for models since machines cannot understand why almost identical visual features have different annotations and require them to make different prediction results. The second one is the long-tail effect which exists objectively in nature. Some of the dominant predicate classes are almost 1,000 times as many as less-frequent ones, leading to a bad performance on those less frequent

predicates. Too many general predicates like “on” in training will lead to insufficient training for less-frequent ones like “eating” and drifting preference away from fine ones such as “parked on”. Some methods, including re-weighting and re-sampling, seem to be a suitable choice. However, due to the hierarchical annotation in the dataset, the improvement seems to be limited according to [47].

When training the deep network, problems like the long-tail effect and mixed-granularity annotation are universal but catastrophic to the deep network training. In contrast, humans seem capable of handling these complicated problems. As shown in cognitive psychology research [15], human beings appear to learn gradually and hierarchically. Coincidentally, the semantic structure of predicates in VG is similar to our real-life naming, consisting of mixed-granularity information. For instance, parents often teach their kids to recognize “bird” first and then go for the specific kinds like “mockingbird” or “cuckoo”. Inspired by this, we realize that it is plausible to design a hierarchical training framework to resolve the abovementioned problems by imitating human learning behavior.

This work proposes a Hierarchical Memory Learning (HML) framework for hierarchical fashion training with the consideration mentioned above. At the very beginning, we cluster predicates and establish a hierarchical tree in Fig. 1 and separate the dataset by the tree layers without any extra manual annotation. To realize hierarchical training, Concept Reconstruction (CR) is used to inherit the previous model’s predicate recognition ability by imitating its output. For a similar purpose, Model Reconstruction (MR) directly fits the parameters in the previous model as a stronger constraint. Under this training scenario, the model gets less chance to confront the previously discussed dilemma and is much easier to train with a relatively small and balanced fraction of predicates.

The proposed HML framework is a general training framework and can train any off-the-shelf SGG model. Fig. 1 shows the scene graph generated by the hierarchical training scenario. The scene graph predicted by the model trained with the HML framework is more comprehensive and fine-grained. The predicted relationships such as “bike-parked on-sidewalk” and “plate-on back of-bike” are more informative and meaningful than “bike-on-sidewalk” and “plate-on-bike”.

The main contributions of this work can be summarized as:

- Inspired by human learning behavior, we propose a novel HML framework, and its generality can be demonstrated by applying it to various classic models.
- We present two new CR and MR constraints to consolidate knowledge from coarse to fine.
- Our HML framework overperforms all existing optimization frameworks. Besides, one common model trained under HML will also be competitive among various SGG methods with the trade-off between fine and coarse prediction.

2 Related Work

2.1 Scene Graph Generation

SGG [54,60] has received increasing attention in the computer vision community because of its potential in various down-stream visual tasks [20,50,57]. Nevertheless, the prerequisite is the generation of fine-grained and informative scene graph. Recent works consider SGG mainly from three perspectives.

Model Design. At the very beginning, some works designed elaborate structures for better feature refinement. [54] leveraged GRUs to pass messages between edges and nodes. [63] explored that the feature of objects and predicates can be represented in low-dimensional space, which inspired works like [21,22,40]. [60] chose BiLSTM for object and predicate context encoding. [48] encoded hierarchical and parallel relationships between objects and carried out a score matrix to find the existence of relationships between objects. Unfortunately, the improvement is limited with elaborate model design alone.

Framework Formulation. Later works tried to design the optimization framework to improve the model performance further. Based on causal inference, [47] used Total Direct Effect for unbiased SGG. [43] proposed an energy-based constraint to learn predicates in small numbers. [59] formulated the predicate tree structure and used tree-based class-balance loss for training. [59] and our work both focus on the granularity of predicates and share some similarities.

Dataset Property. The long-tail effect was particularly pronounced in VG, making studying this problem very important. [7] utilized dynamic frequency for the better training. [10] proposed a novel class-balance sampling strategy to capture entities and predicates distributions. [17] sought a semantic level balance of predicates. [29] used bipartite GNN and bi-level data re-sampling strategy to alleviate the imbalance. However, another problem (mixed-granularity annotation) in the dataset is not fully explored, which inspires this work.

2.2 Long-Tail Learning

Only a few works like [7,10,17,29] cast importance on the long-tail effect in VG. In fact, many long-tail learning strategies can be used in SGG. The previous works tackling the long-tail effect can be roughly divided into three strategies.

Re-sampling. Re-sampling is one of the most popular methods to resolve the class imbalance. Simple methods like random over-sampling and random under-sampling will lead to overfitting the tail and degrading the head. Thus, recent work like [14,23,51,65] monitored optimization process of depending only instance balance.

Cost-sensitive Learning. Cost-sensitive learning realizes classes balance by adjusting loss for different classes during training. [8,31,42] leveraged label frequency to adjust loss and prediction during the training. [45] regarded one positive sample as a negative sample for other classes in softmax or sigmoid cross-entropy loss calculation. Other works [4,24] tried to handle the long-tail problem by adjusting distances between representation features and the model classifier

for different classes. [14] used mean prediction scores to monitor and guide class-level margin adjustment. [9] used the ordinal margin to maintain discriminative representation, while variational margin attempts to suppress imbalance in the head.

Transfer Learning. Transfer Learning helps to transfer information or knowledge from head to tail and enhance models' performances. [33,58] proposed a guiding feature in the head to augment tail learning. [52] learned to map few-shot model parameters to many-shot ones for better training. Works like [16,30,35] helped to distill knowledge directly from the head to tail.

3 Approach

We will first introduce how to automatically construct a hierarchical predicate tree via clustering (Sec. 3.1). And then turn back to explain our HML framework in (Sec. 3.2), along with loss formulation for CR (Sec. 3.3) and MR (Sec. 3.4).

3.1 Automatic Construction of Predicate Tree

In order to form a predicate tree for our training scenario, we firstly embed all 50 predicates in the dataset into feature vectors with the pre-trained word representation model in [36]. After that, motivated by reporting bias [37], we cluster predicates into different groups and do some pruning (e.g., eliminating the group with a single predicate which will be added to the last layer). We finally pick up the top-K frequent predicates within each group as the first K layers of the tree.

As for clustering, we choose the traditional distributed word embedding (i.e., DWE) algorithm [36] instead of Bert [11] and ELMo [39], since we wish to eliminate the context from objects or subjects which can provide extra information [61] to the predicate embedding. We iterate through all 50 predicates to cluster. The first predicate is automatically divided into the first group and record its embedding vector to be the initial value of first group representation $R_1 = DWE(x_1)$. As for the following ones, we calculate the cosine distance among all current group representations:

$$SS^{ij} = \frac{R_i \cdot DWE(x_j)}{\|R_i\| \times \|DWE(x_j)\|}, \quad (1)$$

where SS^{ij} is the semantic similarity between current iterated predicate x_j and i^{th} group representations R_i . $DWE(x)$ represents distributed word embedding function on predicate. Max cosine distance SS_{max}^{ij} will be recorded and compared with the empirical threshold T_{SS} whose setting is mentioned in Sec. 4.3. If SS^{ij} is larger than the threshold, current iterated predicate x_j will be added into the existing group. Otherwise, we create a new group for it. The group representations will be updated in the following rule:

$$\begin{cases} R_{N+1} = DWE(x_j), SS_{max}^{ij} < T_{SS} \\ R_i = \frac{n \cdot R_i + DWE(x_j)}{n+1}, SS_{max}^{ij} \geq T_{SS} \end{cases}, \quad (2)$$

where N is the current number of groups and n is the number of predicates in the i^{th} group.

After clustering, the most frequent predicates are assigned to the first layer, the second frequent predicates are assigned to the second layer, etc. It is worth noticing that during this clustering, some human actions such as “looking at”, “playing”, “says”, “eating”, and “walking in” will become a single group as one single predicate. We automatically divide them into the last layer since those human action predicates are almost 100 to 1000 times less than predicates in the other layer. The most suitable number of layers depends on the dataset itself. Sec. 4.6 analyzes the best layer number for the VG dataset.

3.2 Hierarchical Memory Learning Framework

Most SGG models comprise two steps. In the beginning, an image is fed into an ordinary object detector to get bounding boxes, corresponding features of these regions, and the logits over each object class. These detection results are used to predict the scene graph in the next step. The feature of a node is initialized by box features, object labels, and position. Some structures like LSTM [41,60] are used to refine nodes’ features through passing and incorporating the messages. After that, the object labels are obtained directly by refined feature, while the predicates are predicted from the union features refined by the structures of BiLSTM [60], BiTreeLSTM [41], GRU [12], or GNN [29].

Nevertheless, most of the models are still trained on the whole dataset at one time, making the task still challenging. To address long-tail effect and mixed-granularity annotation, we believe it is a better solution to disentangle semantic-confusing predicate classes by dealing with general relationships (e.g., “on”, “has”) and informative ones (e.g., “sitting on”, “using”) separately in different stages. In this training scenario, the model in its stage can only focus on a small fraction of predicates with relatively similar granularity and then congregate the knowledge from previous stages step by step.

Since the SGG task is similar to the human learning pattern, absorbing knowledge from coarse to fine, it is natural to model how humans learn. Given the model trained in the previous stage, the current training model needs to gain the ability to do well in previous classes while learning how to deal with new classes. A naive way is to sample some images in the last stage for review. Nevertheless, this strategy is unsuitable for our situation since it reintroduces mixed-granularity predicates. Thus, for better knowledge consolidation, we adopt **Concept Reconstruction (CR)** and **Model Reconstruction (MR)** which will be further explained in Sec. 3.3 and Sec. 3.4. CR will be adopted to decrease the distance between the prediction logits produced by two models. This process is similar to how human students imitate teachers to solve problems. Human brain cortical areas have different functional networks [15]. It is the same for the parameters in an SGG model. MR respects the hypothesis that different parameters in a model serve for different relationships recognition. As is shown in Fig. 2, in the second to N^{th} stage, the model will fit the prediction and parameters for knowledge passing. At the same time, the gradient and parameters’ change will

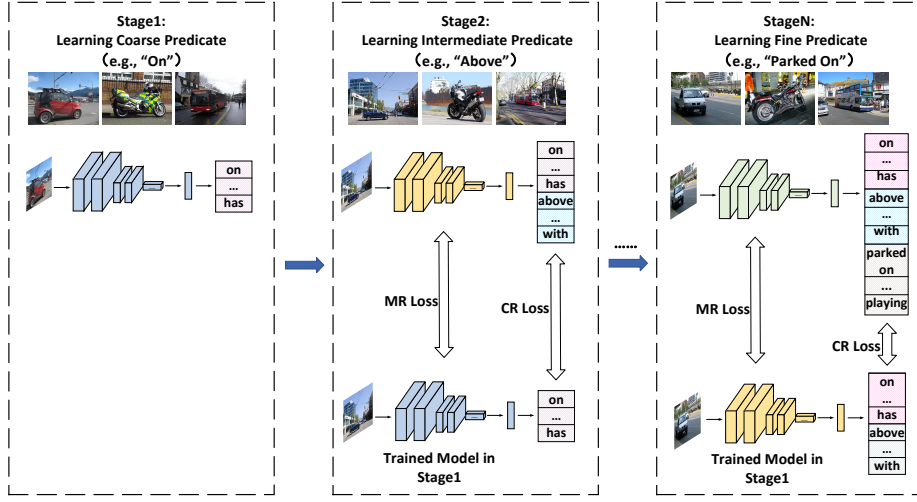


Fig. 2: **Overview of HML Framework.** We train the model in a coarse to fine fashion. In each step, the model calculates CR and MR for knowledge assimilation. Meanwhile, the importance scores and empirical Fisher Information Matrix are calculated after updating the model. The importance score and empirical Fisher Information Matrix are passed down at the end of each stage. For the VG dataset, we set stage number to be 2 and explain in Sec. 4.6.

be stored for the online update of empirical Fisher Information Matrix (Sec. 3.4) and importance scores (Sec. 3.4).

Does a deep network have parameter redundancy? Some earlier work did answer this question. Hinton *et al.* [19] came up with knowledge distillation for the first time to compress and transfer knowledge from a complicated model to a more compact one that is easier to deploy. Moreover, it was verified in [3] that a cumbersome model can be compressed into a compact one. Based on these works, we assume that the whole model comprises many parameters, and these parameters or “activated” neurons in an SGG network should target specific predicate classes, as is shown in Fig. 1. To verify this assumption, we compare the mean of importance scores, which will be further illustrated in Sec. 3.4 and verified in supplementary material from the experimental perspective, of all the parameters in each layer and find out that the values vary between different stages. This mechanism is similar to how the human brain works. Each region in the brain has its’ own function and works together to finish complex tasks [15]. After learning through all stages, the model will classify all classes with fine-grained preference.

The total loss for the HML framework is given by:

$$\ell = \ell_{new} + \alpha \ell_{CR} + \beta \ell_{MR}, \quad (3)$$

where $\alpha = \frac{N_{old}}{N_{new}}$, $\beta = \lambda \frac{N_{new} + N_{old}}{N_{new}}$, N_{new} is the number of new predicate classes, N_{old} is the number of old predicate classes and λ is a hyper-parameter. ℓ_{CR} is Concept Reconstruction loss and ℓ_{MR} is Model Reconstruction loss.

ℓ_{new} in Eq. (3) is Class-Balance loss [8] and used to learn current stage predicates:

$$\ell_{new} = -W_B \sum_{i=1}^C y_i \log \frac{e^{z_i}}{\sum_{j=1}^C e^{z_j}}, \quad (4)$$

where z represents the output of the model, y is the one-hot ground-truth label vector, and C is the number of predicate classes. $W_B = \frac{1-\gamma}{1-\gamma^{n_i}}$, γ denotes the hyper-parameter that represents the sample domain, and n_i denotes number of predicate i in current stage.

3.3 Concept Reconstruction Loss

In order to prevent activation drift [3], CR is applied. It is an implicit way to keep the prediction of previous predicates from drifting too much. Thus, we need to find the distance between two prediction from different stages of the same visual relationship and reduce it. The CR loss can be represented by:

$$\ell_{CR}(X_n, Z_n) = \frac{\sum_{i=1}^{N_n} \sum_{j=1}^{C_{old}} (\text{Softmax}(x_n^{ij}) - \text{Softmax}(z_n^{ij}))^2}{N_n}, \quad (5)$$

where x_n^i and z_n^i are the output logits vector for the prediction. N_n is the number of outputs. We choose L2 distance [2] as the distance metric. Compared with the traditional loss function such as L1 loss and cross-entropy loss with the soft label, L2 loss is a stronger constraint but sensitive to outliers. Fortunately, since the training process is coarse to fine, the representations will not drastically deviate, making L2 loss practical. With the consideration as mentioned earlier, L2 distance is used in CR, receiving better performance in experiments. This is also verified in [64].

In a word, CR is used to help the current model learn how to make the same prediction as to the previous model.

3.4 Model Reconstruction Loss

The parameters of the model determine the ability to recognize visual relationships. Thus, it is a more straightforward way to learn directly from parameters. A feasible solution is to determine which parameters are crucial in previous stage classification and fit them with greater attention in the following stage.

KL-divergence is a mathematical statistics measure of how a probability distribution is different from another one [27]. KL-divergence, denoted as in the form of $D_{KL}(p_\theta || p_{\theta+\Delta\theta})$, can also be used to calculate the difference of the conditional likelihood between a model at θ and $\theta + \Delta\theta$. Since changes of parameters are subtle (i.e., $\Delta\theta \rightarrow 0$) during the optimization, we will get the second-order

of Taylor approximation of KL-divergence, which is also the distance in Riemannian manifold induced by Fisher Information Matrix [28] and can be written as $D_{KL}(p_\theta || p_{\theta+\Delta\theta}) \approx \frac{1}{2} \Delta\theta^\top F_\theta \Delta\theta$, where the F_θ is known as empirical Fisher Information Matrix [38] at θ and the approximate will be proved in supplementary material, is defined as:

$$F_\theta = \mathbb{E}_{(\mathbf{x}, \mathbf{y}) \sim D} \left[\left(\frac{\partial \log p_\theta(\mathbf{y}|\mathbf{x})}{\partial \theta} \right) \left(\frac{\partial \log p_\theta(\mathbf{y}|\mathbf{x})}{\partial \theta} \right)^\top \right], \quad (6)$$

where D is the dataset and $p_\theta(y|x)$ is the log-likelihood. However, in practice, if a model has P parameters, it means $F_\theta \in R^{P \times P}$, and it is computationally expensive. To solve this, we compromise and assume parameters are all independent, making F_θ diagonal. Then the approximation of KL-divergence looks like:

$$D_{KL}(p_\theta || p_{\theta+\Delta\theta}) \approx \frac{1}{2} \sum_{i=1}^P F_{\theta_i} \Delta\theta_i^2, \quad (7)$$

where θ_i is the i^{th} parameters of the model and P is the total number of the model.

During the training, F_θ will be updated in each iteration, following the rule of:

$$F_\theta^t = \frac{F_\theta^t + (t-1) \cdot F_\theta^{t-1}}{t}, \quad (8)$$

where t is the number of iterations.

Although the empirical Fisher Information Matrix captures static information of the model, it fails to capture the influence of each parameter during optimization in each stage. Thus, we adopt the method in [62] to search for essential parameters. Intuitively, if the value of a parameter changes a little in a single step, but it contributes a lot to the decrease of the loss, we think it is essential, at least for the current task. So, the importance of a parameter during an interval (from t to Δt) can be represented as:

$$\Omega_{raw}(\theta_i) = \sum_t^{t+\Delta t} \frac{\Delta \ell_t^{t+1}(\theta_i)}{\frac{1}{2} F_{\theta_i}^t (\theta_i(t+1) - \theta_i(t))^2 + \epsilon}, \quad (9)$$

$$\Omega_t^{t+\Delta t}(\theta_i) = \sigma \left(\log_{10} \frac{P \times \Omega_{raw}(\theta_i)}{\sum_{i=1}^P \Omega_{raw}(\theta_i)} \right), \quad (10)$$

where σ is the sigmoid function, numerator $\Delta \ell_t^{t+1}(\theta_i)$ is the change of loss caused by θ_i in one step, $\epsilon > 0$ aims to avoid the change of loss $\Delta\theta_i = \theta_i(t+1) - \theta_i(t) = 0$, and the denominator is the KL-divergence of θ_i between t and $t+1$ (i.e., one step).

To be more specific, $\Delta \ell_t^{t+1}(\theta_i)$ represents how much contribution does θ_i make to decrease the loss. Since the optimization trajectory is hard to track, to find the change in loss caused by θ_i , we need to figure out a way to split the

overall loss form into the sum of each parameter’s contributions. The solution is first-order Taylor approximation:

$$\ell(\theta(t+1)) - \ell(\theta(t)) \approx - \sum_{i=1}^P \sum_{t=t}^{t+1} \frac{\partial \ell}{\partial \theta_i} (\theta_i(t+1) - \theta_i(t)) = - \sum_{i=1}^P \Delta \ell_t^{t+1}(\theta_i), \quad (11)$$

where $\frac{\partial \ell}{\partial \theta_i}$ is the gradient of θ_i and $\theta_i(t+1) - \theta_i(t)$ is the value change of θ_i during a single step. If $\ell(\theta(t+1)) - \ell(\theta(t)) > 0$, we set $\Delta \ell_t^{t+1}(\theta_i)$ to be 0, since we consider only when the loss become smaller, a step of optimization can be regarded as effective.

The empirical Fisher Information Matrix is used twice. The first is to calculate the difference of probability distributions of two models in different stages, and the second is to find the changes of a model in a nearby iteration within a single stage.

So, after figuring out how important each parameter is, the MR loss can be written as:

$$\ell_{MR} = \frac{\sum_{i=1}^P \left(F_{\theta_i}^{k-1} + (\Omega_{t_0}^{t_0+\Delta t})^{k-1}(\theta_i) \right) (\theta_i^k - \theta_i^{k-1})^2}{P}, \quad (12)$$

where P is the number of parameters for relationship prediction in the model and k represents current stage. $F_{\theta_i}^{k-1}$ and $(\Omega_{t_0}^{t_0+\Delta t})^{k-1}$ are both calculated in previous stage.

Fisher Information Matrix F_θ and importance scores $\Omega_{t_0}^{t_0+\Delta t}$ are used to represent the importance of parameters from static and dynamic perspectives, respectively.

4 Experiment

4.1 Dataset and Model

Dataset. In the SGG task, we choose Visual Genome (VG) [26] as the dataset for both training and evaluation. It comprises 75k object categories and 40k predicate categories. However, due to the scarcity of over 90% predicates are less than ten instances, we applied the widely accepted split in [6,41,60], using the 150 highest frequency objects categories and 50 predicate categories. The training set is set to be 70%, and the testing set is 30%, with 5k images from the training set for finetuning. [47].

Model. We evaluate HML framework on three models and follow the setting in [46]:

- MOTIFS [60]: Using a bidirectional LSTM to create a context representation of objects with semantic features.
- Transformer [13,49]: Using multi-head transformer encoders to refine feature and gather information.
- VCTree [41]: Constructing binary tree, and using bidirectional TreeLSTM for encoding and decoding.

Model	Framework	Predicate Classification			Scene Graph Classification			Scene Graph Detection		
		mR@20	mR@50	mR@100	mR@20	mR@50	mR@100	mR@20	mR@50	mR@100
Transformer [49]	Baseline	14.13	17.87	19.38	8.23	10.14	10.77	6.25	8.50	10.05
	CogTree [59]	22.90	28.40	31.00	13.00	15.70	16.70	7.90	11.10	12.70
	BPL+SA [17]	26.70	31.90	34.20	15.70	18.50	19.40	11.40	14.80	17.10
	HML(Ours)	27.35	33.25	35.85	15.71	19.10	20.43	11.43	14.96	17.67
MOTIFS [60]	Baseline	12.54	15.89	17.19	7.38	9.09	9.66	5.34	7.32	8.56
	EBM [44]	14.17	18.02	19.53	8.18	10.22	10.98	5.66	7.72	9.27
	SG [25]	14.50	18.50	20.20	8.90	11.20	12.10	6.40	8.30	9.20
	TDE [47]	18.50	25.50	29.10	9.80	13.10	14.90	5.80	8.20	9.80
	CogTree [59]	20.90	26.40	29.00	12.10	14.90	16.10	7.90	10.40	11.80
	DLFE [7]	22.10	26.90	28.80	12.80	15.20	15.90	8.60	11.70	13.80
	BPL+SA [17]	24.80	29.70	31.70	14.00	16.50	17.50	10.70	13.50	15.60
	HML(Ours)	30.10	36.28	38.67	17.07	20.80	22.10	10.84	14.56	17.27
VCTree [48]	Baseline	13.36	16.81	18.08	8.48	10.54	11.21	5.90	8.17	9.62
	EBM [44]	14.20	18.19	19.72	10.40	12.54	13.45	5.67	7.71	9.10
	SG [25]	15.00	19.20	21.10	9.30	11.60	12.30	6.30	8.10	9.00
	TDE [47]	18.40	25.40	28.70	8.90	12.20	14.00	6.90	9.30	11.10
	CogTree [59]	22.00	27.60	29.70	15.40	18.80	19.90	7.80	10.40	12.10
	DLFE [7]	20.80	25.30	27.10	15.80	18.90	20.00	8.60	11.80	13.80
	BPL+SA [17]	26.20	30.60	32.60	17.20	20.10	21.20	10.60	13.50	15.70
	HML(Ours)	31.04	36.90	39.21	20.46	25.03	26.82	10.06	13.71	16.31

(a) Comparison between HML framework and various optimization frameworks.

Model+Framework	Predicate Classification		Scene Graph Classification		Scene Graph Detection		Mean@50/100
	mR@50/100	R@50/100	mR@50/100	R@50/100	mR@50/100	R@50/100	
MOTIFS-TDE [47]	25.5/29.1	46.2/51.4	13.1/14.9	27.7/29.9	8.2/9.8	16.9/20.3	22.9/25.9
MOTIFS-DLFE [7]	26.9/28.8	52.5/54.2	15.2/15.9	32.3/33.1	11.7/13.8	25.4/29.4	27.3/29.2
Transformer-CogTree [59]	28.4/31.0	38.4/39.7	15.7/16.7	22.9/23.4	11.1/12.7	19.5/21.7	22.7/24.2
PCPL [55]	35.2/37.8	50.8/52.6	18.6/19.6	27.6/28.4	9.5/11.7	14.6/18.6	26.1/28.1
DT2-ACBS [10]	35.9/39.7	23.3/25.6	24.8/27.5	16.2/17.6	22.0/24.4	15.0/16.3	22.9/25.2
Transformer-HML(Ours)	33.3/35.9	45.6/47.8	19.1/20.4	22.5/23.8	15.0/17.7	15.4/18.6	25.2/27.4
MOTIFS-HML(Ours)	36.3/38.7	47.1/49.1	20.8/22.1	26.1/27.4	14.6/17.3	17.6/21.1	27.1/29.3
VCTree-HML(Ours)	36.9/39.2	47.0/48.8	25.0/26.8	27.0/28.4	13.7/16.3	17.6/21.0	27.9/30.1

(b) A more comprehensive comparison between HML framework and various SOTAs.

Table 1: Result of Relationship Retrieval mR@K [48] and R@K.

4.2 Evaluation

Sub-Tasks. SGG can be further divided into three sub-tasks:

- **Predicate Classification:** given images, object bounding boxes, and object labels, predicting the relationship labels between objects.
- **Scene Graph Classification:** given images and object bounding boxes, predicting object labels and relationship labels between objects.
- **Scene Graph Detection:** localizing objects, recognizing objects, and predicting the relationships between them directly from images.

Relationship Recall. We choose **Mean Recall@K (mR@K)** [48] as a metric to evaluate the performance of SGG models. As is shown in [47], regular Recall@K (R@K) will lead to the reporting bias due to the imbalance that lies

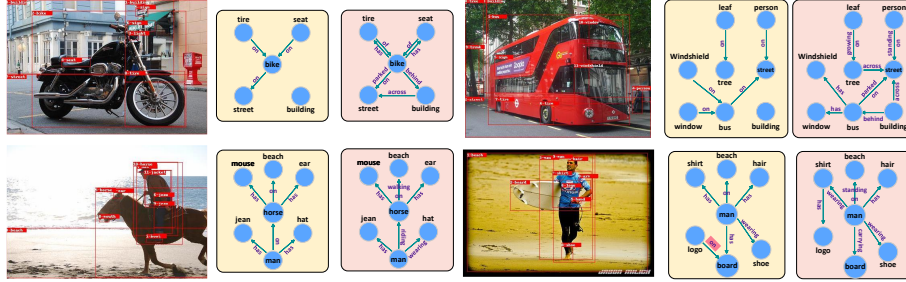


Fig. 3: **Qualitative Results.** Basic model generates yellow scene graphs and pink ones are predicted by the same basic model under HML training.

in the data (e.g., a model that only correctly classifies top 5 frequent predicates can reach 75% of Recall@100). Thus, we introduce **Mean@K** which calculates the average score of all three sub-tasks R@K and mR@K under identical K. Mean@K is a metric to evaluate overall performance on both R@K and mR@K. We will further explain the reason and necessity of using this metric in the supplementary material.

4.3 Implementation Details

Object Detector. We pre-train a Faster-RCNN with ResNeXt-101-FPN [53] and freeze the previously trained weight during the SGG training period. The final detector reached 28 mAP on the VG test set.

Relationship Predictor. The backbone of baseline models is replaced with an identical one and hierarchical trained in the same setting. We set the batch size to 12 and use SGD optimizer with an initial learning rate of 0.001, which will be decayed by 10 after the validation performance plateaus. The experiment was carried out on NVIDIA TITAN RTX GPUs.

Hierarchical Predicate Tree Construction. For Visual Genome (VG), the whole predicates are split into two disjoint subsets (tasks) following the construction in Sec. 3.1. The threshold is set to be $T_{SS} \in [0.65, 0.75]$ in Eq. (2). Too high predicates cannot cluster together, while too low make lots of predicates mix together. During the sampling for the training set, only when all the predicates in one image come from the same layer of the tree will this image be selected into the training set.

Hierarchical Training. In our experiment, two identical models will be trained separately in two stages. Moreover, the first model will be initialized randomly, and the previous stage models will not be used to initialize the following model. If not, the model will meet the intransigence [5] problem. Besides, we set the number of max iterations to 8000 and 16000 in the first and second stages. Nevertheless, models will usually converge around 8000 in both stages. The λ in an overall loss is set to 0.5 for the best performance as is shown in Tab. 3a.

Model	CR	MR	Predicate Classification					
			mR@20	mR@50	mR@100	R@20	R@50	R@100
Transformer [49]			14.13	17.87	19.38	58.79	65.29	67.09
	✓		24.14	29.27	31.22	29.1	36.16	38.57
		✓	23.32	29.34	32.20	38.80	46.48	48.87
	✓	✓	27.35	33.25	35.85	38.81	45.61	47.78
MOTIFS [60]			12.54	15.89	17.19	59.12	65.45	67.20
	✓		24.69	30.00	32.79	33.92	41.34	43.95
		✓	21.56	27.43	30.05	44.30	51.87	54.14
	✓	✓	30.10	36.28	38.67	40.52	47.11	49.08
VCTree [48]			13.36	16.81	18.08	59.76	65.48	67.49
	✓		22.32	29.34	32.20	27.86	35.21	37.73
		✓	22.84	28.94	31.48	43.81	51.40	53.74
	✓	✓	31.04	36.90	39.21	40.28	46.47	48.36

Table 2: **Ablation on CR and MR.** We explore the functionality of CR loss and MR loss.

4.4 Quantitative Study

In Tab. 1a, our HML framework can consistently outperform the existing frameworks under various fundamental models. By applying the HML framework on different models, we notice that models will drastically improve the Mean Recall for all three sub-tasks. The improvement scale is similar with different models such as Motif, Transformer, and VCTree. In Tab. 1b, we compare HML with various SOTAs which report R@K and mR@K at the same time. After calculating Mean@K, it turns out that HML can not only make the fine-grained prediction (demonstrated by mR@K) but keep clear boundaries of general predicates (demonstrated by R@K).

In Tab. 2, we notice a vital decrease in R@K. After analyzing each predicate, we figure out that the decline mainly comes from the drop of general predicates such as “on” and “has”. After HML training, the mR@100 of “on” and “has” dropped from 79.98 to 31.01 and 81.22 to 58.34. It is the model preference on the fine-grained prediction that causes this decrease. Thus, we replace the fine-grained one with a general one and recalculate R@100, and the results of “on” and “has” re-bounce to be 71.72 and 86.91, respectively. Works like [7,10,47,55,59] compared in Tab. 1b can also make relatively fine-grained prediction (i.e., relatively high mR@K) but all suffer from decrease of R@K partially due to the reason mentioned above.

4.5 Qualitative Study

We visualize the qualitative result generated by original MOTIFS and MOTIFS trained with the HML framework in Fig. 3. Compared with the original model,

layer	Predicates Classification			time (hr)	λ	Predicates Classification		
	mR@20	mR@50	mR@100			mR@20	mR@50	mR@100
1	12.54	15.89	17.19	17.85	0.00	25.24	31.95	34.44
2	30.10	36.28	38.67	29.43	0.25	30.97	35.91	37.88
3	25.24	31.95	34.44	44.65	0.50	30.10	36.28	38.67
4	15.66	21.96	25.32	60.13	0.75	29.73	34.36	36.79
					1.00	29.20	33.47	35.69

(a) Ablation of Layer Number

(b) Ablation of λ Table 3: **Ablation on MOTIFS.** We explore different numbers of layer and λ with MOTIFS on the performance of Mean Recall@K.

the model trained under HML will make informative predictions such as “parked on”, “growing on”, “standing on”, “riding”, and “walking on” instead of general one “on”. Also, our model will tend to make fine-grained predictions such as “wearing” and “carrying” instead of “has”. Besides, since we train a model hierarchically, the model will obtain the ability to capture tail part predicates such as “building-across-street” and position predicates such as “building-behind-bus” and “tree-behind-bus”.

4.6 Ablation Studies

CR and MR. We further explore the contributions of each term in our overall loss. In the SGG task, Recall@K and Mean Recall@K [48] restrict mutually with each other. Recall@K represents how well the model does for the head part of the predicate classes. Thus, it reflects how well a mode can imitate the previous model. On the contrary, Mean Recall@K [48] evaluates the model’s overall performance. If we want to figure out the functionality of the knowledge consolidation term in the loss, it is reasonable to adopt Recall@K since two terms of knowledge reconstruction aim to prevent the model from forgetting previous knowledge. According to Tab. 2, if we add CR and MR separately, mR@K will get constant improvement. However, only when CR and MR are used simultaneously will we get the highest mR@K and prevent R@K from dropping too much. Also, after comparing the second and third row of each model on R@K, it is obvious that MR is a more powerful constraint than CR.

Layer Number. The number of layers (i.e., stage) depends on how many top-K frequent predicates we pick up after clustering. We conduct experiments in Tab. 3a on different layers and figure out 2 is suitable for the VG dataset, mainly due to small predicate classes number and limited granularity variance. HML training indeed needs more time to complete training during multi-stage training. Nevertheless, the increase ratio (125%) of model performance is way more significant than the one (65%) of training time. More time analysis will be shown in the supplementary material. All experiments were carried out on one

identical GPU, and the calculation of the total is based on the average time of several identical trainings.

Hyperparameter λ . In order to figure out the effect of λ on the performance of the model, we set 5 values in ablation to $\lambda \in \{0, 0.25, 0.50, 0.75, 1.00\}$ in Tab. 3b. λ represents how much information will be passed down to the next stage. If λ is too high, the new model will stick to original classes without learning new classes. In contrast, low λ can not guarantee effective information passing. Based on our experiment, $\lambda = 0.5$ is suitable for the HML framework on VG.

5 Conclusion

We propose a general framework to enable SGG models to make the fine-grained prediction. In addition to the objective long-tail effect in the dataset, we uncover mixed-granularity predicates caused by subjective human annotation. The similarity between the human hierarchical learning pattern and the SGG problem is obvious under this condition. Based on that, we designed the HML framework with two new constraints (i.e., CR and MR) for efficient training. We observe that the HML framework can improve performance compared to the traditional training fashion models and achieves new state-of-the-art.

References

1. Agrawal, A., Batra, D., Parikh, D., Kembhavi, A.: Don't just assume; look and answer: Overcoming priors for visual question answering. In: CVPR. pp. 4971–4980 (2018) [2](#)
2. Ba, L.J., Caruana, R.: Do deep nets really need to be deep? NIPS (2014) [8](#)
3. Bucilua, C., Caruana, R., Niculescu-Mizil, A.: Model compression. In: KDD. pp. 535–541 (2006) [7](#), [8](#)
4. Cao, D., Zhu, X., Huang, X., Guo, J., Lei, Z.: Domain balancing: Face recognition on long-tailed domains. In: CVPR. pp. 5671–5679 (2020) [4](#)
5. Chaudhry, A., Dokania, P.K., Ajanthan, T., Torr, P.H.: Riemannian walk for incremental learning: Understanding forgetting and intransigence. In: ECCV. pp. 532–547 (2018) [12](#)
6. Chen, L., Zhang, H., Xiao, J., He, X., Pu, S., Chang, S.F.: Counterfactual critic multi-agent training for scene graph generation. In: ICCV. pp. 4613–4623 (2019) [10](#)
7. Chiou, M.J., Ding, H., Yan, H., Wang, C., Zimmermann, R., Feng, J.: Recovering the unbiased scene graphs from the biased ones. In: ACMMM. pp. 1581–1590 (2021) [2](#), [4](#), [11](#), [13](#)
8. Cui, Y., Jia, M., Lin, T.Y., Song, Y., Belongie, S.: Class-balanced loss based on effective number of samples. In: CVPR. pp. 9268–9277 (2019) [4](#), [8](#)
9. Deng, Z., Liu, H., Wang, Y., Wang, C., Yu, Z., Sun, X.: Pml: Progressive margin loss for long-tailed age classification. In: CVPR. pp. 10503–10512 (2021) [5](#)
10. Desai, A., Wu, T.Y., Tripathi, S., Vasconcelos, N.: Learning of visual relations: The devil is in the tails. In: ICCV. pp. 15404–15413 (2021) [4](#), [11](#), [13](#)
11. Devlin, J., Chang, M., Lee, K., Toutanova, K.: BERT: pre-training of deep bidirectional transformers for language understanding. In: Burstein, J., Doran, C., Solorio, T. (eds.) NAACL. pp. 4171–4186. Association for Computational Linguistics (2019) [5](#)
12. Dhingra, N., Ritter, F., Kunz, A.: Bgt-net: Bidirectional gru transformer network for scene graph generation. In: CVPR. pp. 2150–2159 (2021) [6](#)
13. Dosovitskiy, A., Beyer, L., Kolesnikov, A., Weissenborn, D., Zhai, X., Unterthiner, T., Dehghani, M., Minderer, M., Heigold, G., Gelly, S., et al.: An image is worth 16x16 words: Transformers for image recognition at scale. ICLR (2020) [10](#)
14. Feng, C., Zhong, Y., Huang, W.: Exploring classification equilibrium in long-tailed object detection. In: ICCV. pp. 3417–3426 (2021) [4](#), [5](#)
15. Genon, S., Reid, A., Langner, R., Amunts, K., Eickhoff, S.B.: How to characterize the function of a brain region. Trends in cognitive sciences **22**(4), 350–364 (2018) [3](#), [6](#), [7](#)
16. Goodfellow, I.J., Mirza, M., Xiao, D., Courville, A., Bengio, Y.: An empirical investigation of catastrophic forgetting in gradient-based neural networks. In: ICLR (2014) [5](#)
17. Guo, Y., Gao, L., Wang, X., Hu, Y., Xu, X., Lu, X., Shen, H.T., Song, J.: From general to specific: Informative scene graph generation via balance adjustment. In: ICCV. pp. 16383–16392 (2021) [2](#), [4](#), [11](#)
18. Hendricks, L.A., Burns, K., Saenko, K., Darrell, T., Rohrbach, A.: Women also snowboard: Overcoming bias in captioning models. In: ECCV. pp. 771–787 (2018) [1](#)
19. Hinton, G., Vinyals, O., Dean, J.: Distilling the knowledge in a neural network. CoRR (2015) [7](#)

20. Hudson, D.A., Manning, C.D.: Gqa: A new dataset for real-world visual reasoning and compositional question answering. In: CVPR. pp. 6700–6709 (2019) 4
21. Hung, Z., Mallya, A., Lazebnik, S.: Contextual translation embedding for visual relationship detection and scene graph generation. TPAMI **43**(11), 3820–3832 (Nov 2021) 4
22. Ji, G., He, S., Xu, L., Liu, K., Zhao, J.: Knowledge graph embedding via dynamic mapping matrix. In: Knowledge graph embedding via dynamic mapping matrix. pp. 687–696 (Jul 2015) 4
23. Kang, B., Xie, S., Rohrbach, M., Yan, Z., Gordo, A., Feng, J., Kalantidis, Y.: Decoupling representation and classifier for long-tailed recognition. ICLR (2020) 4
24. Khan, S., Hayat, M., Zamir, S.W., Shen, J., Shao, L.: Striking the right balance with uncertainty. In: CVPR. pp. 103–112 (2019) 4
25. Khandelwal, S., Suhail, M., Sigal, L.: Segmentation-grounded scene graph generation. In: ICCV. pp. 15879–15889 (2021) 11
26. Krishna, R., Zhu, Y., Groth, O., Johnson, J., Hata, K., Kravitz, J., Chen, S., Kalantidis, Y., Li, L.J., Shamma, D.A., et al.: Visual genome: Connecting language and vision using crowdsourced dense image annotations. IJCV **123**(1), 32–73 (2017) 10
27. Kullback, S., Leibler, R.A.: On information and sufficiency. The annals of mathematical statistics **22**(1), 79–86 (1951) 8
28. Lee, J.M.: Riemannian manifolds: an introduction to curvature, vol. 176. Springer Science & Business Media (2006) 9
29. Li, R., Zhang, S., Wan, B., He, X.: Bipartite graph network with adaptive message passing for unbiased scene graph generation. In: CVPR. pp. 11109–11119 (2021) 4, 6
30. Li, T., Wang, L., Wu, G.: Self supervision to distillation for long-tailed visual recognition. In: ICCV. pp. 630–639 (2021) 5
31. Lin, T.Y., Goyal, P., Girshick, R., He, K., Dollár, P.: Focal loss for dense object detection. In: ICCV. pp. 2980–2988 (2017) 4
32. Lin, T.Y., Maire, M., Belongie, S., Hays, J., Perona, P., Ramanan, D., Dollár, P., Zitnick, C.L.: Microsoft coco: Common objects in context. In: ECCV. pp. 740–755. Springer (2014) 2
33. Liu, J., Sun, Y., Han, C., Dou, Z., Li, W.: Deep representation learning on long-tailed data: A learnable embedding augmentation perspective. In: CVPR. pp. 2970–2979 (2020) 5
34. Manjunatha, V., Saini, N., Davis, L.S.: Explicit bias discovery in visual question answering models. In: CVPR. pp. 9562–9571 (2019) 2
35. McCloskey, M., Cohen, N.J.: Catastrophic interference in connectionist networks: The sequential learning problem. In: Psychology of learning and motivation, vol. 24, pp. 109–165. Elsevier (1989) 5
36. Mikolov, T., Grave, E., Bojanowski, P., Puhersch, C., Joulin, A.: Advances in pre-training distributed word representations. In: LREC (2018) 5
37. Misra, I., Lawrence Zitnick, C., Mitchell, M., Girshick, R.: Seeing through the human reporting bias: Visual classifiers from noisy human-centric labels. In: CVPR. pp. 2930–2939 (2016) 5
38. Pascanu, R., Bengio, Y.: Revisiting natural gradient for deep networks. ICLR (2014) 9
39. Peters, M.E., Neumann, M., Iyyer, M., Gardner, M., Clark, C., Lee, K., Zettlemoyer, L.: Deep contextualized word representations. In: NAACL. pp. 2227–2237. Association for Computational Linguistics (2018) 5

40. Peyre, J., Laptev, I., Schmid, C., Sivic, J.: Detecting unseen visual relations using analogies. In: ICCV. pp. 1981–1990 (2019) [4](#)
41. Rebuffi, S.A., Kolesnikov, A., Sperl, G., Lampert, C.H.: icarl: Incremental classifier and representation learning. In: CVPR (July 2017) [6](#), [10](#)
42. Ren, J., Yu, C., Ma, X., Zhao, H., Yi, S., et al.: Balanced meta-softmax for long-tailed visual recognition. NIPS **33**, 4175–4186 (2020) [4](#)
43. Suhail, M., Mittal, A., Siddiquie, B., Broaddus, C., Eledath, J., Medioni, G., Sigal, L.: Energy-based learning for scene graph generation. In: CVPR. pp. 13936–13945 (2021) [2](#), [4](#)
44. Suhail, M., Mittal, A., Siddiquie, B., Broaddus, C., Eledath, J., Medioni, G., Sigal, L.: Energy-based learning for scene graph generation. In: CVPR. pp. 13936–13945 (2021) [11](#)
45. Tan, J., Wang, C., Li, B., Li, Q., Ouyang, W., Yin, C., Yan, J.: Equalization loss for long-tailed object recognition. In: CVPR. pp. 11662–11671 (2020) [4](#)
46. Tang, K.: A scene graph generation codebase in pytorch (2020), <https://github.com/KaihuaTang/Scene-Graph-Benchmark.pytorch> [10](#)
47. Tang, K., Niu, Y., Huang, J., Shi, J., Zhang, H.: Unbiased scene graph generation from biased training. In: CVPR. pp. 3716–3725 (2020) [2](#), [3](#), [4](#), [10](#), [11](#), [13](#)
48. Tang, K., Zhang, H., Wu, B., Luo, W., Liu, W.: Learning to compose dynamic tree structures for visual contexts. In: CVPR. pp. 6619–6628 (2019) [2](#), [4](#), [11](#), [13](#), [14](#)
49. Vaswani, A., Shazeer, N., Parmar, N., Uszkoreit, J., Jones, L., Gomez, A.N., Kaiser, L., Polosukhin, I.: Attention is all you need. In: NIPS. pp. 5998–6008 (2017) [10](#), [11](#), [13](#)
50. Wang, S., Wang, R., Yao, Z., Shan, S., Chen, X.: Cross-modal scene graph matching for relationship-aware image-text retrieval. In: WACV. pp. 1508–1517 (2020) [4](#)
51. Wang, T., Li, Y., Kang, B., Li, J., Liew, J., Tang, S., Hoi, S., Feng, J.: The devil is in classification: A simple framework for long-tail instance segmentation. In: ECCV. pp. 728–744. Springer (2020) [4](#)
52. Wang, Y.X., Ramanan, D., Hebert, M.: Learning to model the tail. NIPS **30** (2017) [5](#)
53. Xie, S., Girshick, R., Dollár, P., Tu, Z., He, K.: Aggregated residual transformations for deep neural networks. In: CVPR. pp. 1492–1500 (2017) [12](#)
54. Xu, D., Zhu, Y., Choy, C.B., Fei-Fei, L.: Scene graph generation by iterative message passing. In: CVPR. pp. 5410–5419 (2017) [1](#), [4](#)
55. Yan, S., Shen, C., Jin, Z., Huang, J., Jiang, R., Chen, Y., Hua, X.S.: Pcppl: Predicate-correlation perception learning for unbiased scene graph generation. In: ACMML. pp. 265–273 (2020) [11](#), [13](#)
56. Yang, J., Lu, J., Lee, S., Batra, D., Parikh, D.: Graph r-cnn for scene graph generation. In: ECCV. pp. 670–685 (2018) [2](#)
57. Yang, X., Tang, K., Zhang, H., Cai, J.: Auto-encoding scene graphs for image captioning. In: CVPR. pp. 10685–10694 (2019) [1](#), [4](#)
58. Yin, X., Yu, X., Sohn, K., Liu, X., Chandraker, M.: Feature transfer learning for face recognition with under-represented data. In: CVPR. pp. 5704–5713 (2019) [5](#)
59. Yu, J., Chai, Y., Wang, Y., Hu, Y., Wu, Q.: Cogtree: Cognition tree loss for unbiased scene graph generation. In: IJCAI. pp. 1274–1280 (2020) [4](#), [11](#), [13](#)
60. Zellers, R., Yatskar, M., Thomson, S., Choi, Y.: Neural motifs: Scene graph parsing with global context. In: CVPR. pp. 5831–5840 (2018) [2](#), [4](#), [6](#), [10](#), [11](#), [13](#)
61. Zellers, R., Yatskar, M., Thomson, S., Choi, Y.: Neural motifs: Scene graph parsing with global context. In: CVPR. pp. 5831–5840 (2018) [5](#)
62. Zenke, F., Poole, B., Ganguli, S.: Continual learning through synaptic intelligence. In: ICML. pp. 3987–3995 (2017) [9](#)

- 63. Zhang, H., Kyaw, Z., Chang, S.F., Chua, T.S.: Visual translation embedding network for visual relation detection. CVPR pp. 3107–3115 (2017) [4](#)
- 64. Zhang, J., Zhang, J., Ghosh, S., Li, D., Tasci, S., Heck, L., Zhang, H., Kuo, C.C.J.: Class-incremental learning via deep model consolidation. In: WACV. pp. 1131–1140 (2020) [8](#)
- 65. Zhang, X., Wu, Z., Weng, Z., Fu, H., Chen, J., Jiang, Y.G., Davis, L.S.: Videolt: Large-scale long-tailed video recognition. In: ICCV. pp. 7960–7969 (2021) [4](#)

Hierarchical Memory Learning for Fine-Grained Scene Graph Generation - Appendix

Abstract. The supplementary document is organized as follows: Sec. 1 gives a brief proof of approximate KL-Divergence; Sec. 2 explains the rationality and necessity of Mean@K; Sec. 3 verifies the fine-grained prediction ability by visualizing the qualitative results on each predicate; Sec. 4 analyzes the variance of importance scores of parameters in the deep network; Sec. 5 provides a more comprehensive analysis about the training time.

1 Proof of Approximate KL-Divergence

Formally, the KL-Divergence [1] can be defined as:

$$D_{KL}(p_\theta(\mathbf{y}|\mathbf{x})||p_{\theta+\Delta\theta}(\mathbf{y}|\mathbf{x})) = \mathbb{E}_{(\mathbf{y},\mathbf{x}) \sim D} [\log p_\theta(\mathbf{y}|\mathbf{x}) - \log p_{\theta+\Delta\theta}(\mathbf{y}|\mathbf{x})]. \quad (1)$$

With the second Taylor Expansion of $\log p_{\theta+\Delta\theta}(\mathbf{y}|\mathbf{x})$ at θ , we can get:

$$\log p_{\theta+\Delta\theta}(\mathbf{y}|\mathbf{x}) \approx \log p_\theta(\mathbf{y}|\mathbf{x}) + \Delta\theta^\top \frac{\partial \log p_\theta(\mathbf{y}|\mathbf{x})}{\partial \theta} + \frac{1}{2} \Delta\theta^\top \frac{\partial^2 \log p_\theta(\mathbf{y}|\mathbf{x})}{\partial \theta^2} \Delta\theta. \quad (2)$$

Then, substitute Eq. (2) into Eq. (1) and we get the approximate KL-Divergence:

$$\begin{aligned} D_{KL}(p_\theta(\mathbf{y}|\mathbf{x})||p_{\theta+\Delta\theta}(\mathbf{y}|\mathbf{x})) &\approx \mathbb{E}_{(\mathbf{x},\mathbf{y}) \sim D} [\log p_\theta(\mathbf{y}|\mathbf{x})] - \mathbb{E}_{(\mathbf{x},\mathbf{y}) \sim D} [\log p_{\theta+\Delta\theta}(\mathbf{y}|\mathbf{x})] \\ &\quad - \Delta\theta^\top \mathbb{E}_{(\mathbf{x},\mathbf{y}) \sim D} \left[\frac{\partial \log p_\theta(\mathbf{y}|\mathbf{x})}{\partial \theta} \right] - \frac{1}{2} \Delta\theta^\top \mathbb{E}_{(\mathbf{x},\mathbf{y}) \sim D} \left[\frac{\partial^2 \log p_\theta(\mathbf{y}|\mathbf{x})}{\partial \theta^2} \right] \Delta\theta. \end{aligned} \quad (3)$$

In Eq. (3), the first order partial derivative can be eliminated by:

$$\begin{aligned} \mathbb{E}_{(\mathbf{x},\mathbf{y}) \sim D} \left[\frac{\partial \log p_\theta(\mathbf{y}|\mathbf{x})}{\partial \theta} \right] &= \mathbb{E}_{\mathbf{x} \sim D} \left[\sum_{\mathbf{y}} p_\theta(\mathbf{y}|\mathbf{x}) \frac{\partial \log p_\theta(\mathbf{y}|\mathbf{x})}{\partial \theta} \right] \\ &= \mathbb{E}_{\mathbf{x} \sim D} \left[\sum_{\mathbf{y}} p_\theta(\mathbf{y}|\mathbf{x}) \frac{1}{p_\theta(\mathbf{y}|\mathbf{x})} \frac{\partial p_\theta(\mathbf{y}|\mathbf{x})}{\partial \theta} \right] \\ &= \mathbb{E}_{\mathbf{x} \sim D} \left[\frac{1}{\partial \theta} \sum_{\mathbf{y}} \partial p_\theta(\mathbf{y}|\mathbf{x}) \right] \\ &= \mathbb{E}_{\mathbf{x} \sim D} [0] = 0. \end{aligned} \quad (4)$$

In addition, the second order partial derivative in Eq. (3) can be replaced by Fisher Matrix F_θ :

$$\begin{aligned} \mathbb{E}_{(\mathbf{x}, \mathbf{y}) \sim D} \left[-\frac{\partial^2 \log p_\theta(\mathbf{y}|\mathbf{x})}{\partial \theta^2} \right] &= \mathbb{E}_{(\mathbf{x}, \mathbf{y}) \sim D} \left[-\frac{1}{p_\theta(\mathbf{y}|\mathbf{x})} \frac{\partial^2 p_\theta(\mathbf{y}|\mathbf{x})}{\partial \theta^2} \right] \\ &+ \mathbb{E}_{(\mathbf{x}, \mathbf{y}) \sim D} \left[\left(\frac{\partial \log p_\theta(\mathbf{y}|\mathbf{x})}{\partial \theta} \right) \left(\frac{\partial \log p_\theta(\mathbf{y}|\mathbf{x})}{\partial \theta} \right)^\top \right] = 0 + F_\theta. \end{aligned} \quad (5)$$

By substituting Eq. (4) and Eq. (5), we get the approximate KL-Divergence:

$$\begin{aligned} D_{KL}(p_\theta(\mathbf{y}|\mathbf{x}) || p_{\theta+\Delta\theta}(\mathbf{y}|\mathbf{x})) &\approx \frac{1}{2} \Delta\theta^\top \mathbb{E}_{(\mathbf{x}, \mathbf{y}) \sim D} \left[-\frac{\partial^2 \log p_\theta(\mathbf{y}|\mathbf{x})}{\partial \theta^2} \right] \Delta\theta \\ &= \frac{1}{2} \Delta\theta^\top F_\theta \Delta\theta. \end{aligned} \quad (6)$$

2 Rationality and Necessity of Metric Mean@K

With an identical visual relationship in an image, people tend to annotate the relationships with high-frequent predicates instead of more informative ones [2]. For example, “dog-on-bench” is more likely to be annotated instead of “dog-sitting on-bench”. Because of this labeling phenomenon, if a model has a fine-grained prediction preference, it will have a bad performance on the “head part” (e.g., “on” and “has”). The reasonable and fine-grained predictions will be regarded as mistakes, which leads to the reporting bias of Recall@K (R@K). Thus, taking R@K as the primary evaluation metric is not plausible. For a better evaluation, [3] adopted mean Recall@K (mR@K) as the primary metric for the first time.

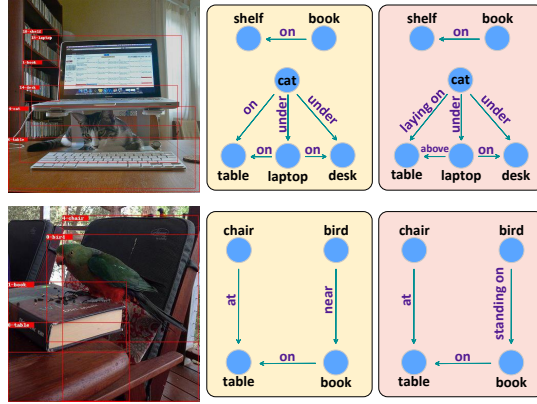


Fig. 1. Image with both position and verb as different granularity. Yellow scene graph is predicted by VCTree [4], while pink one is predicted by VCTree-HML.

Unfortunately, there is an intriguing fact that lies in our semantic expressions. Some kinds of objects with verb property typically have more fine-grained labeling, while other kinds of objects typically have position labeling. We can find several specific occasions like Fig. 1. The relationships between daily life objects are mostly positional, such as “book-on-shelf” or “laptop-on-desk”. In this circumstance, “standing on” or “growing on” is not suitable. In contrast, animals like “bird” and “cat” or humans including “kid” and “man” have more verb relationships such as “sitting on” and “laying on”. Hence, considering $mR@K$ alone is also not very comprehensive.

Since $mR@K$ and $R@K$ restrict mutually, any methods with higher $mR@K$ will get less $R@K$, vice versa. With the consideration above, we adopt $Mean@K$, which calculates the average score of $mR@K$ and $R@K$ under an identical K to evaluate our HML further and provide a fair comparison.

3 Verification of Fine-Grained Prediction Ability

For better analysis and comparison, we compare the improvement of $R@100$ [5] on each predicate, respectively. The experiments were carried out on three models that are used in body part of our paper: Motif [6], Transformer [7,8], and VCTree [4].

In Figs. 2 to 4, we visualize the qualitative results of traditional training model and model with our HML on each predicate. We do not use the name of predicates for simplicity. Instead, we rank all predicates in the order of frequency, and the X-axis number represents each predicate’s ranking. It is worth noticing that the performance improvements are impressive. Some “tail part” predicates that can not be correctly recognized in the original training framework drastically rise. Besides, the reason for the decline in the “head part” including “on” and “has” has been discussed in the body part of our paper.

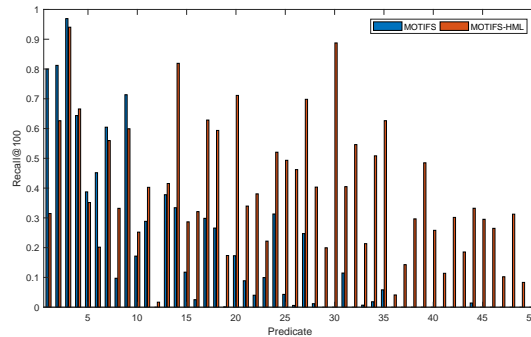


Fig. 2. Motif: Recall@100 [5] on Predicate Classification for all 50 predicates.

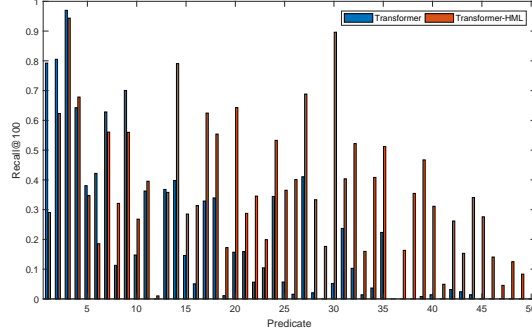


Fig. 3. Transformer: Recall@100 [5] on Predicate Classification for all 50 predicates.

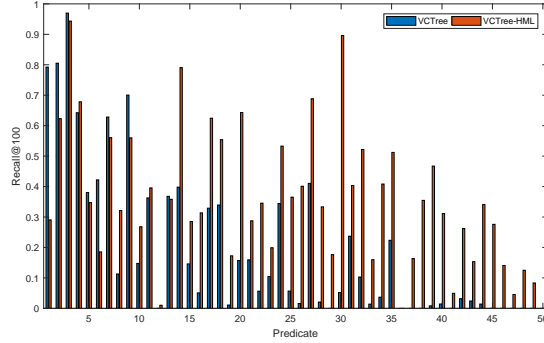


Fig. 4. VCTree: Recall@100 [5] on Predicate Classification for all 50 predicates.

4 Variance of Importance Scores of Parameters

As illustrated in the Model Reconstruction Loss section, an importance score is an efficient way to evaluate each parameter’s importance in a model. To verify our assumption that the parameters in the target for different predicate classes, we visualize Figs. 5 to 7. For simplicity, we omit backbone layers and only pick up the weights concerning relation prediction. We first calculate the fractions of each parameter in the first and second stages like:

$$Frac(p_n) = \frac{p_n^1}{p_n^2}, \quad (7)$$

where n represents n^{th} one of all parameters and superscripts 1 and 2 represent the stage number. Then find the mean of $Frac(p_n)$ of each layer (the number of the X-axis in the figure represents the layer number). The result of Figs. 5 to 7, shows that the importance scores of different parameters in each layer fluctuate a lot, verifying the assumption that different models parameters specialize in different tasks (i.e., different predicates).

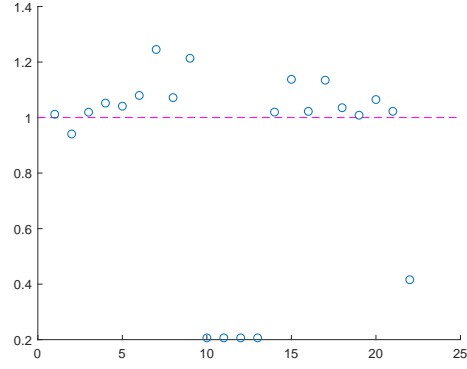


Fig. 5. The mean of importance scores in each relation prediction layer of MOTIFS [6].

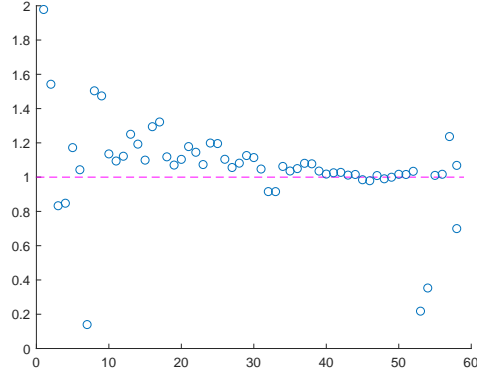


Fig. 6. The mean of importance scores in each relation prediction layer of Transformer [7,8].

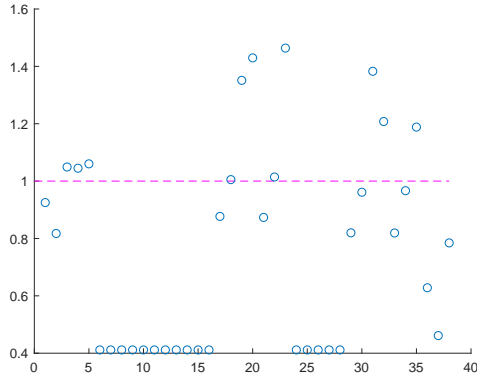


Fig. 7. The mean of importance scores in each relation prediction layer of VCTree [4].

5 Time Analysis

Intuitively, our HML tends to be extremely time-consuming due to hierarchical learning. In order to explore the computational complexity of our HML, we compare all competitive methods that have publicly released the source code in the last two years. We train all the methods under the same GPU computing environment and record the running times. We further analyze the training time per image on MOITFS with different frameworks for a more comprehensive study. Because of the different training conditions, it is hard to compare all methods fairly. For instance, some methods can be trained quickly for every image, but it takes longer to converge.

As is shown in Sec. 5, indeed, our HML spends more than twice the training time on one image than other methods. However, the property of the HML framework is worth noticing. In the HML, a model is trained under the guidance of a well-trained model and within a relatively balanced and small fraction of data. Therefore, it takes fewer iterations for a model under the HML to converge, making the increase of the training not that significant.

All the experiments were carried out on one identical NVIDIA Tesla V100 GPU to pursue a fair comparison. Due to the limited memory of our GPU, we can not fully carry out identical experiment settings in [9] set batch-size to be 12 instead of the original 48 setting.

Model+Framework	mR@50/100	Time/img (s)	Overall Time (hr)
MOTIFS [6]	15.9/17.2	0.101	8.636
MOTIFS-TDE [3]	25.5/29.1	0.105	9.542
MOTIFS-CogTree [10]	26.4/29.0	0.124	8.487
MOTIFS-DLFE [12]	26.9/28.8	0.103	7.731
MOTIFS-BPL-SA [11]	29.7/31.7	0.211	11.135
PCPL [9]	35.2/37.8	0.119	8.163
MOTIFS-HML (Ours)	36.9/39.2	0.223	10.933

Table 1. Time evaluation on Predicate Classification. We compare different methods with our HML of training time per image and overall time.

References

1. Kullback, S., Leibler, R.A.: On information and sufficiency. *The annals of mathematical statistics* **22**(1), 79–86 (1951) [1](#)
2. Misra, I., Lawrence Zitnick, C., Mitchell, M., Girshick, R.: Seeing through the human reporting bias: Visual classifiers from noisy human-centric labels. In: CVPR. pp. 2930–2939 (2016) [2](#)
3. Tang, K., Niu, Y., Huang, J., Shi, J., Zhang, H.: Unbiased scene graph generation from biased training. In: CVPR. pp. 3716–3725 (2020) [2](#), [6](#)
4. Rebuffi, S.A., Kolesnikov, A., Sperl, G., Lampert, C.H.: icarl: Incremental classifier and representation learning. In: CVPR (July 2017) [2](#), [3](#), [5](#)
5. Tang, K., Zhang, H., Wu, B., Luo, W., Liu, W.: Learning to compose dynamic tree structures for visual contexts. In: CVPR. pp. 6619–6628 (2019) [3](#), [4](#)
6. Zellers, R., Yatskar, M., Thomson, S., Choi, Y.: Neural motifs: Scene graph parsing with global context. In: CVPR. pp. 5831–5840 (2018) [3](#), [5](#), [6](#)
7. Vaswani, A., Shazeer, N., Parmar, N., Uszkoreit, J., Jones, L., Gomez, A.N., Kaiser, L., Polosukhin, I.: Attention is all you need. In: NIPS. pp. 5998–6008 (2017) [3](#), [5](#)
8. Dosovitskiy, A., Beyer, L., Kolesnikov, A., Weissenborn, D., Zhai, X., Unterthiner, T., Dehghani, M., Minderer, M., Heigold, G., Gelly, S., et al.: An image is worth 16x16 words: Transformers for image recognition at scale. ICLR (2020) [3](#), [5](#)
9. Yan, S., Shen, C., Jin, Z., Huang, J., Jiang, R., Chen, Y., Hua, X.S.: Pcpl: Predicate-correlation perception learning for unbiased scene graph generation. In: ACMMM. pp. 265–273 (2020) [6](#)
10. Yu, J., Chai, Y., Wang, Y., Hu, Y., Wu, Q.: Cogtree: Cognition tree loss for unbiased scene graph generation. In: IJCAI. pp. 1274–1280 (2020) [6](#)
11. Guo, Y., Gao, L., Wang, X., Hu, Y., Xu, X., Lu, X., Shen, H.T., Song, J.: From general to specific: Informative scene graph generation via balance adjustment. In: ICCV. pp. 16383–16392 (2021) [6](#)
12. Chiou, M.J., Ding, H., Yan, H., Wang, C., Zimmermann, R., Feng, J.: Recovering the unbiased scene graphs from the biased ones. In: ACMMM. pp. 1581–1590 (2021) [6](#)